LA-UR- 09-00912

Approved for public release;
distribution is unlimited.

Title:	Higher-order symplectic Born-Oppenheimer molecular dynamics
Author(s):	Anders Niklasson, Anders Odell, Anna Delin, Borje Johansson, Nicolas Bock, Matt Challacombe
Intended for:	Journal of Chemical Physics

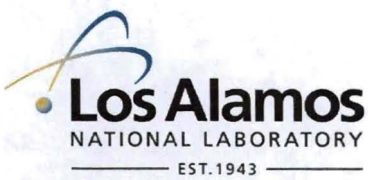

Form 836 (7/06)

LA-UR 08-XXXX

Higher-order symplectic Born-Oppenheimer molecular dynamics

Anders Odell *, Anna Delin, and Börje Johansson
Applied Materials Physics, Department of Materials Science and Engineering, Royal Institute of Technology, SE-100 44 Stockholm, Sweden

Nicolas Bock, Matt Challacombe, and Anders M. N. Niklasson †
Theoretical Division, Los Alamos National Laboratory, Los Alamos, New Mexico 87545
(Dated: January 19, 2009)

The extended Lagrangian formulation of time-reversible Born-Oppenheimer molecular dynamics (TR-BOMD) [Niklasson et. al. Phys. Rev. Lett. vol. 100, p. 123004, 2008; Phys. Rev. Lett. vol. 97, p. 123001, 2006] enables the use of geometric integrators in the propagation of both the nuclear and the electronic degrees of freedom on the Born-Oppenheimer potential energy surface. Different symplectic integrators up to the *6th* order have been adapted and optimized to TR-BOMD in the framework of *ab initio* self-consistent-field theory. It is shown how the accuracy can be significantly improved compared to a conventional Verlet integration at the same level of computational cost, in particular for the case of very high accuracy requirements.

PACS numbers: 71.15.Pd,31.15.Ew,31.15.Qg,34.10.+x

I. INTRODUCTION

In *ab initio* molecular dynamics the forces on the particles are calculated from the laws of quantum mechanics without empirical parameters [1]. Approximations to the many-particle problem that are used includes density functional theory (DFT), Hartree-Fock (HF) theory and their extensions [2–4]. The Born-Oppenheimer approximation [5] allows for the separation of nuclear and electronic degrees of freedom and the forces are calculated at the electronic ground state [6]. This ensures an adiabatic propagation of the system. However, the evaluation of the forces at each time step involves a computationally demanding self-consistent-field (SCF) optimization of the electronic solution. The number of iterations required to converge the solution may range from ten to hundreds depending on the system. One way to decrease the required number of iterations is to propagate the electronic solution between time steps. This means that some combination of the electronic solutions from previous time steps are used as an initial guess in the SCF optimization. Propagation typically reduce the required number of iterations by an order of magnitude [1, 7–11]. Often only $1-3$ SCF cycles are required. The problem with propagating the electronic solution is that small errors are inherited between time steps, causing a systematic global energy drift and with an unphysical behaviour of the phase space [7, 8, 12]. The only way up till recently to reduce the energy drift was to increase the number of iterations in the SCF loop, forcing the electronic solution closer to the adiabatic surface. This basically removes the inheritance between steps, but greatly increases the computational cost. Another way to solve this problem would be to propagate the electronic solution in a time-reversible way. Time reversible integrators are well known from classical MD to give stable dynamics without a systematic energy drift [13]. This however, can not be done in a straightforward way because of the irreversible and non-linear nature of the SCF optimization. Recently, it was possible to overcome this problem with the construction of Time-reversible Born-Oppenheimer MD.

Time-reversible Born-Oppenheimer MD (TR-BOMD) facilitates simulation without a systematic long-term drift in the energy even under incomplete SCF convergence [12]. TR-BOMD can be described by an extended Lagrangian formulation [14]. This allows for the use of higher-order symplectic integration schemes orginally developed in classical MD and celestial dynamics [13, 15–18]. Symplectic integration of the electronic solution enables highly efficient simulations while keeping a rigorous control over physical properties.

The purpose of this paper is to present and explore the use of higher-order symplectic integration schemes in Time-reversible Born-Oppenheimer MD and to study their efficiency and behaviour under incomplete SCF convergence. Ideally, we would like to identify "the best" scheme. We have implemented several different symplectic integrators up to 6th order in the *ab initio*-code MondoSCF [19]. The different symplectic integration schemes are analysed with respect to stability and accuracy. They are optimized for stability under incomplete SCF convergence and minimal total energy error fluctuations. The different schemes are investigated for small well controlled test systems and their properties are analysed in order to find the optimal symplectic integration scheme for various accuracy requirements.

In section II we explain the theoretical framework of Time-reversible Born-Oppenheimer MD in its extended Lagrangian formulation. In section III we discuss different integration schemes and explain higher-order sym-

*Email: odell@mse.kth.se
†Email: amn@lanl.gov

plectic integrators and their optimization for TR-BOMD. In section IV we present the calculations for different test systems and analyse and discuss the behaviour of the integrators under different circumstances. The last section (V) contains a summary and discussion of the work.

II. TIME-REVERSIBLE BORN-OPPENHEIMER MOLECULAR DYNAMICS

The equations of motion for regular Born-Oppenheimer molecular dynamics can be derived from the BO Lagrangian:

$$\mathcal{L}^{\mathrm{BO}}(\mathbf{R},\dot{\mathbf{R}}) = \frac{1}{2}\sum_k M_k \dot{R}_k^2 - U_{\mathrm{SCF}}[\mathbf{R};D] \qquad (1)$$

where $\mathbf{R} = \{R_k\}$ and M_k are the nuclear coordinates and masses. U_{SCF} is the self consistent total electronic energy from Hartree-Fock or density functional theory. D is the self consistent ground state solution for the elctronic degrees of freedom which can be represented by the one-particle density matrix, the electronic density, the wave functions or the Hamiltonian. In this work D denotes the densiy matrix in an orthogonal basis-set representation. The Euler-Lagrange equations,

$$\frac{d}{dt}\frac{\partial \mathcal{L}}{\partial \dot{\mathbf{R}}} = \frac{\partial \mathcal{L}}{\partial \mathbf{R}}, \qquad (2)$$

gives the equations of motion for the dynamical variables in the Lagrangian. The Euler-Lagrange equations of motion can be numerically integrated using time reversible and/or symplectic schemes that preserve physical properties of the system. Unfortunately, the density matrix D in the BO Lagrangian in Eq. (1) does not occur as a dynamical variable. D is not an independent dynamical variable since it is given uniquely from $\mathbf{R}$, if the SCF optimization is exact. If the electronic degrees of freedom could be included as dynamical variables in the Lagrangian, they could be integrated in a systematic way. This trick was successfully applied two decades ago by Car and Parinello [21], simply by neglecting the SCF optimization and adding a kinetic energy term and orthogonality constraints to the electronic degrees of freedom. The Car-Parrinello method has the drawback of an artificial electronic mass that has to be tuned for different systems. Only in the limit of vannishing values of the mass parameter is the theory exact. The largest possible time-step that can be used in the integration is determined by the evolution of the electronic degrees of freedom, which is very fast if the electronic mass is small. The Car-Parrinello method therefore typically requires time steps that are very small compared to the evolution of the nuclear degrees of freedom. Also no optimization of the electronic degrees of freedom is performed. Thus the nuclear degrees of freedom do not evolve on the BO potential energy surface. However, statistical averages are often accurate [1, 22].

The solution in TR-BOMD to systematically propagate the electronic degrees of freedom, while still staying on the BO surface, without breaking the time reversal symmetry, is to add an auxiliary dynamical variable P to the Born-Oppenheimer Lagrangian that has the same form as the self-consistent electronic solution D. P evolves in an extended potential centered around the ground state solution D, but without any self consistent optimization. The most straightforward choise is to let the auxiliary variable P move in a harmonic potential around D. This can be described by the extended Born-Oppenheimer (XBO) Lagrangian,

$$\mathcal{L}^{\mathrm{XBO}}(\mathbf{R},\dot{\mathbf{R}},P,\dot{P}) = \mathcal{L}^{\mathrm{BO}} + \frac{\mu}{2}Tr[\dot{P}^T\dot{P}] - \frac{\mu\omega^2}{2}Tr[(D-P)^T(D-P)] \qquad (3)$$

Here Tr denotes the trace of a matrix. The auxiliary variables P and $\dot{P}$ are included with a kinetic term and a harmonic potential term. The parameter μ is a fictitious mass parameter for the electronic degrees of freedom and the parameter ω is a fictitious frequency for the extended harmonic potential. The parameter ω determines the curvature of the harmonic potential that P evolves in. The higher curvature of the potential, i.e. larger ω, the closer P will stay to D. The value for ω can be optimized with respect to stability for a given time step and integration scheme. This will be further discussed in section III C.

The time evolution of the dynamical system described by the extended Lagrangian $\mathcal{L}^{XBO}$ is determined by the Euler-Lagrange equations of motion:

$$M_k\ddot{R}_k = -\frac{\partial U_{\mathrm{SCF}}[\mathbf{R};D]}{\partial R_k} - \mu\omega^2 Tr[(D-P)\partial D/\partial R_k], \qquad (4)$$

$$\mu\ddot{P} = \mu\omega(D-P). \qquad (5)$$

To avoid the technical problem with the density matrix derivative in Eq. (4) and the arbitrary choice of μ, we take the limit $\mu \to 0$. In this case $\mathcal{L}^{XBO} \to \mathcal{L}^{BO}$. This is ideal, since P should not affect the dynamics of the nuclear degrees of freedom. The dynamics is now determined by

$$M_k\ddot{R}_k = -\frac{\partial U_{\mathrm{SCF}}[\mathbf{R};D]}{\partial R_k}, \qquad (6)$$

$$\ddot{P} = \omega(D-P). \qquad (7)$$

Equation (6) is the regular BOMD equation of motion for the nuclear coordinates. It shows that the forces on the nuclei are calculated at the self consistent electronic ground state D. The nuclei therefore propagate on the BO potential energy surface and the BO total energy is a constant of the motion. Equation (7) is the equation of motion for the auxiliary electronic degrees of freedom, which is the key equation of TR-BOMD. It is independent of μ, and no fictitious mass parameter has

to be included in the propagation. Although we call the Lagrangian in Eq. (3) *extended*, we prefer to call the varibale P *auxiliary* since it does not change the nuclear equations of motion. This is in contrast to other extended Lagrangian formulations of *ab initio* MD [21, 23, 24].

Since the auxiliary electronic degrees of freedom $P(t)$ evolve in a harmonic potential centered around the self-consistent solutions $D(t)$ in Eq. (3), the auxiliary density matrix $P(t)$, and $D(t)$ will stay close together. We can therefore use $P(t)$ as an efficient initial guess to $D(t)$ in the iterative SCF optimization,

$$D(t) = \mathrm{SCF}[\mathbf{R}(t), P(t)]. \tag{8}$$

If $P(t)$ is integrated by a time-reversible integration scheme, the evolution of $D(t)$ will also be time-reversible. The nuclear forces are then calculated with an underlying time reversible propagation of the electronic degrees of freedom. With this scheme we therefore get a time-reversible propagation for both the nuclear and the electronic degrees of freedom, which avoids the problem of energy drift and unphysical behaviour in regular Born-Oppenheimer molecular dynamics. We refer to dynamical simulations based on Eq. (6), (7) and (8) as TR-BOMD, also when we integrate the equations of motion with algorithms that are not necessarily time-reversible, e.g. several of the symplectic schemes in this study.

TR-BOMD does not remove the local truncation error, but the accumulation of error in the total energy is not systematic. In figure 1 the total energy over time is shown for three different integration schemes. The TR-BOMD

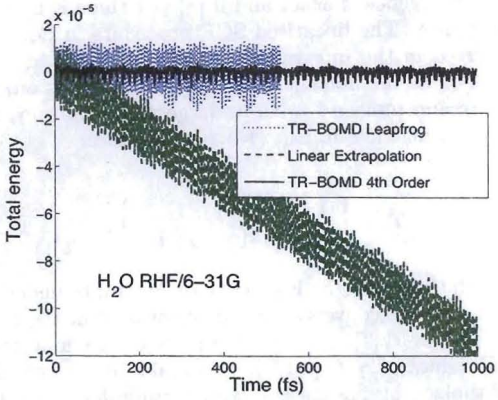

FIG. 1: Total energy for a H_2O molecule with threee different methods. The number of SCF cycles are 4 for all methods and the time step is chosen for each method so that the computational cost is the same.

schemes in Fig. 1 clearly conserves the total energy globally, while the conventional linear extrapolation shows a systematic drift in the energy. It is also shown that the higher order symplectic integrator (4th order) has a smaller total energy fluctuation amplitude (error amplitude) than the symplectic Verlet integrator (2nd order). The error amplitude E_{err} is defined as half the absolute difference between the smallest total energy E_{min} and the largest total energy E_{max},

$$E_{err} = \frac{E_{max} - E_{min}}{2}. \tag{9}$$

Equation (9) has a meaning only when there is no global drift in the total energy. We will use it as a measure of the local truncation error that occur because of the application of a finite time step δt in the integration of Eqs. (6) and (7).

III. INTEGRATION SCHEMES

The solutions to Eqs. (6) and (7) can be approximated with numerical integration methods. Many different algorithms exist that approximate the solutions with different levels of accuracy and stability. Of interest in this article are geometric integrators, which preserves geometric properties of the exact flow of the differential equations. All the methods investigated in this work belong to symplectic integrators, a subclass of geometric integrators, which will be adapted for the numerical solution of the Euler-Lagrange equations of motion as they occur in TRBOMD.

A. Conventional Verlet scheme

If we apply the time-reversible Verlet scheme [20] to the integration of the electronic degrees of freedom in Eq. (7) we get

$$P(t+\delta t) = 2P(t) - P(t-\delta t) + \delta t^2\omega^2\big(D(t) - P(t)\big). \tag{10}$$

If we choose the dimensionless factor $\delta t^2\omega^2 = 2$ this propagation is identical to the linear integration scheme in the original formulation of time-reversible Born-Oppenheimer molecular dynamics [12],

$$P(t+\delta t) = 2D(t) - P(t-\delta t). \tag{11}$$

B. Higher-order symplectic schemes

In higher-order integration schemes the local truncation error scales as a higher order of the time step δt. A nth order scheme scales as $O(\delta t^n)$. To achieve the higher order of accuracy the integration over each time step is divided into a number of intermediate steps. Symplectic integrators form a class of algorithms for solving Hamiltons equations (or the corresponding Lagrange equations of motion) that preserves the linear symplectic structure

inherent in the phase space representation of the dynamics [30, 31].

For the nuclear coordinates in Eq. (6) a quite general symplectic integration [17, 26] over a time length δt is divided in m steps $(i = 1, 2, \ldots, m)$

$$\begin{aligned} \dot{R}_k(t_i) &= \dot{R}_k(t_{i-1}) + b_i \delta t \ddot{R}_k(t_{i-1}), \\ R_k(t_i) &= R_k(t_{i-1}) + a_i \delta t \dot{R}_k(t_i). \end{aligned} \tag{12}$$

Here

$$\begin{bmatrix} R_k(t_0) \\ \dot{R}_k(t_0) \end{bmatrix} = \begin{bmatrix} R_k(t) \\ \dot{R}_k(t) \end{bmatrix}$$

and

$$\begin{bmatrix} R_k(t+\delta t) \\ \dot{R}_k(t+\delta t) \end{bmatrix} = \begin{bmatrix} R_k(t_m) \\ \dot{R}_k(t_m) \end{bmatrix}.$$

For the electronic degrees of freedom in Eq. (7), for $i = 1, 2, \ldots, m$, and using the variable substitution $\delta t \dot{P}(t) \rightarrow \dot{P}(t)$, the symplectic integration is

$$\begin{aligned} \dot{P}(t_i) &= \dot{P}(t_{i-1}) + b_i \kappa \left(D(t_{i-1}) - P(t_{i-1}) \right), \\ P(t_i) &= P(t_{i-1}) + a_i \dot{P}(t_i), \end{aligned} \tag{13}$$

where $D(t_i) = \mathrm{SCF}[\mathbf{R}(t_i), P(t_i)]$. Here $\kappa = \delta t^2 \omega^2$,

$$\begin{bmatrix} P(t_0) \\ \dot{P}(t_0) \end{bmatrix} = \begin{bmatrix} P(t) \\ \dot{P}(t) \end{bmatrix}$$

and

$$\begin{bmatrix} P(t+\delta t) \\ \dot{P}(t+\delta t) \end{bmatrix} = \begin{bmatrix} P(t_m) \\ \dot{P}(t_m) \end{bmatrix}.$$

Equation (13) can be written in the more compact matrix form that maps the auxiliary dynamical variables between time steps,

$$\begin{bmatrix} \dot{P}(t) \\ P(t) \end{bmatrix} = T_m T_{m-1} \ldots T_1 \begin{bmatrix} \dot{P}(t-\delta t) \\ P(t-\delta t) \end{bmatrix}, \tag{14}$$

where $(i = 1, 2, \ldots, m)$,

$$T_i = \begin{bmatrix} 1 & b_i \kappa [D(t_i) P(t_i)^{-1} - 1] \\ a_i & a_i b_i \kappa [D(t_i) P(t_i)^{-1} - 1] + 1 \end{bmatrix} \tag{15}$$

are the coefficient matrices. Examples of coefficients a_i and b_i for the integrators investigated in this work can be found in table II in Appendix A. We have chosen several different integration schemes up to $6th$ order. Beginning with the lowest order methods they are (with the names used in this paper): The Leapfrog method [26] which is of $2nd$ order and corresponds to the Verlet method, the Optimal 2nd order method [26], the Optimal 3rd order [26], Ruth's 3rd order method[15], Candy's/Forest's 4th order method [27, 28], McLachlan's & Atela's 4th order method [26], Calvo's & Sanz-Serna's 4th order method [29], Blanes' & Moan's 4th order method [25], the 5th order method [26], Blanes' & Moan's 6th order method (Blanes & Moan 1) [25] (Table 3, $E_f = 0.78$), Blanes' & Moan's 6th order method (Blanes & Maon 2) [25] (Table 3, $E_f = 0.63$) ans Yoshida's 6th order method [17]. The chosen set of integrators is a selection from the existing literature. It is not exhaustive, but it is a fairly broad representation of some of the best performing symplectic integrators used in classical molecular dymanics.

C. Optimization under incomplete SCF convergence

Since ω in Eq. (7) can be chosen arbitrarily we can optimize the value of $\kappa = \delta t^2 \omega^2$ for each integrator. The dimensionless constant κ should be set to the largest value that still allows stability for all levels of SCF convergence, since this gives the largest value of ω for a given time step δt. The curvature of the extended harmonic potential, which is determined by ω in Eq. (3) should be as large as possible to ensure that P stays close to D. To analyze the stability of the integrator in Eq. (13) the SCF optimization procedure is linearized around its exact ground state D^*:

$$D = \mathrm{SCF}[P] \approx D^* + \Gamma(P - D^*) \tag{16}$$

Here Γ corresponds to the linearized SCF optimization kernel representing a super matrix acting on the matrix $(P - D^*)$. The largest eigenvalues γ of the matrix Γ will lie in the interval $\gamma \in [-1, 1]$ if at least some convergence can be assumed in the SCF optimization. If $\gamma = 0$ the SCF convergence is exact and if $|\gamma| = 1$ there is no SCF convergence. The linearised SCF procedure in Eq. (16) is inserted in the integration, Eqs. (13),(14) and (15). If we look at the homogeneous part of the equation, i.e. $D^* \equiv 0$, and replace Γ with its largest eigenvalue γ, the coefficient matrices in Eq. (15) take the form

$$T_i = \begin{bmatrix} 1 & b_i \kappa (\gamma - 1) \\ a_i & a_i b_i \kappa (\gamma - 1) + 1 \end{bmatrix}. \tag{17}$$

For the mapping in Eq. (14) to be stable under all degrees of SCF convergence the eigenvalues of the combined matrix $T_m T_{m-1} \ldots T_1$ should lie on the unit circle for all values of $\gamma \in [-1, 1]$. The value for κ can now be optimized by finding the largest value for which the conditions above hold. The optimized κ-values for each integrator is presented in Table I. By chosing the optimal κ-value any small amount of SCF convergence is enough to guarantee stability. This means that, in principle, only one single SCF cycle is necessary, if at least some small amount of SCF convergence is reached. However, larger values of κ than the optimal can be used as long as a sufficient degree of SCF convergence is enforced, i.e. by using more SCF cycles in each step. A larger value of

κ corresponds to a larger curvature of the auxiliary harmonic potential in Eq. (7). In this way the auxiliary density matrix P can be forced closer to the SCF optimized density matrix D. If a smaller value than the optimal is used for κ, stability is still guaranteed but the propagation of the auxiliary density matrix will deviate more from the SCF solution, increasing the error in the nuclear force calculation. In Figure 2 the error amplitude E_{err} in Eq. (9), for different values of κ is shown. We find that the error decreases with increasing κ even

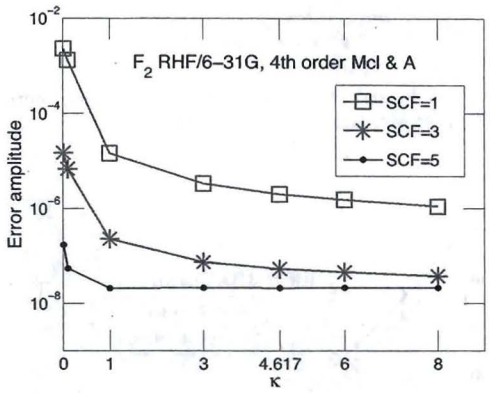

FIG. 2: Error amplitude for a F_2 molecule for different values of κ. The integrator used is McLachlan & Attela's $4th$ order for which the optimized κ-value is 4.617. The time step is $\delta t = 1$ fs.

above the optimal value of $\kappa = 4.617$ when the number of SCF cycles are 1 (SCF = 1) and 3 (SCF = 3). This can however not be expected for a general system since stability is not guaranteed in this regime. For $\kappa > 8$ the calculations were unstable. The error increases when κ decreases because the propagation of the auxiliary electronic degrees of freedom deviates further away from D. When SCF = 5 the error is decreased to the absolute accuracy of the implementation of the code so no improvement can be seen between $\kappa = 1$ and 8. For the hypothetical case of exact SCF convergence there would be no dependence on κ in the error amplitude. We conclude that with a few SCF cycles, or when a good SCF convergence is hard to reach, the accuracy in the integration can be substantially improved by optimizing the κ value. In the opposite case, when a good SCF convergence is easily reached, the accuracy of the propagation is less sensitive to κ.

IV. EXAMPLES AND DISCUSSION

The 12 symplectic integration schemes in table I and II have been systematically tested for three different test systems. The integrators range from $2nd$ to $6th$ order

Name	Ref.	Order	# Steps	κ_{opt}
Leapfrog	[26]	2	1	2
Optimal 2nd	[26]	2	2	2.563
Optimal 3rd	[26]	3	3	10.215
Ruth 3rd	[15]	3	3	3.143
Candy, Forest	[27, 28]	4	4	1.237
McLachlan & Atela	[26]	4	4	4.617
Calvo & Sanz-Serna	[29]	4	5	4.669
Blanes & Moan	[25]	4	7	5.004
5th	[26]	5	6	4.6894
Blanes & Moan 1	[25]	6	12	41.165
Blanes & Moan 2	[25]	6	15	18.911
Yoshida	[17]	6	8	2.574

TABLE I: The symplectic integrators investigated in this work with their order, number of intermediate steps, m, and their optimized κ values.

where the number of intermediate steps, m, range from 1 to 15. The optimized κ-value range between 1.237 and 41.165. The test systems are two diatomic oscillators, the F_2 and the H_2 molecules, and the H_2O molecule. Diatomic molecules are ideal since they exhibit a stable and regular motion. The integrators are tested for the error amplitude E_{err}, Eq. (9), with respect to the length of the time step and to the number of SCF cycles in the SCF optimization.

A. Time step vs Period

Since the integrators have different number of intermediate time steps the computational cost will be different for the same time step. A force evaluation is performed for each intermediate step i in Eqs. (12) and (13), requiring an SCF optimization to get the total electronic energy $U_{\rm SCF}[\mathbf{R}; D]$ in Eq. (6). This force evaluation together with the prior SCF optimization is the most costly part of the simulation. The error amplitude can be plotted against the number of force evaluations per unit time to get a direct comparison between the integrators at the same computational cost. Even more generally, for approximate harmonic oscillators with only one dominant vibration frequency, the error amplitude can be plotted against the number of force evaluations per period. In figure 3 the results for both the F_2 and the H_2 molecules are shown for two different integrators. It is found that the magnitude of the error ultimately depends on the number of force evaluations per period regardless of the system. Whenever possible, the number of force evaluations per period will be used for the comparison of different integrators.

B. Performance over time step

The integrators of $3rd$, $4th$ and $6th$ order are compared in Figs. 4, 5 and 6 for the F_2 molecule with 5 SCF cycles. For a small system like the F_2 molecule this gives a very high degree of SCF convergence. At this level of convergence we can compare the absolute accuracy of the different integrators. The integrator with the smallest error can easily be identified for each order in Figs. 4, 5 and 6. These methods are compared with the Leapfrog, the Optimal 2nd and the $5th$ order method for the F_2 molecule in Fig. 7. In Fig. 8 the same integrators are shown for the H_2O molecule. In this case the period is not uniquely defined so the error amplitude is plotted against the number of force evaluations per unit time. The number of SCF cycles is set to 5, giving a high degree of SCF convergence. The Leapfrog integrator in Figs. 7 and 8 corresponds to the velocity Verlet integrator used in many *ab initio* MD codes for the integration of the nuclear degrees of freedom. The slope of the plots in figure 7 and 8 follows the order of the specific integrator, with the Leapfrog scheme having the least slope and the $6th$ order having the steepest slope. It can be seen that the error amplitude levels out at about 10^{-9} for the F_2 molecule and at about 10^{-8} for the H_2O molecule. This is due to the absolute minimum error of the particular implementation of the current verion of the code, which would be larger for more complex systems. At about 100 force evaluations per period we observe a difference in error amplitude between the Leapfrog and the $6th$ order methods of about three orders of magnitude. Thus, to no extra computational cost the error amplitude can be reduced up to three orders of magnitude for certain time steps. Alternatively, the length of the time step can be increased up to 100 times for this accuracy requirement by using a higher-order symplectic method compared to the Leapfrog algorithm. In the other end of the graph in Figs. (7) and (8), i.e. for long time steps, the lower order methods perform better than the higher order methods.

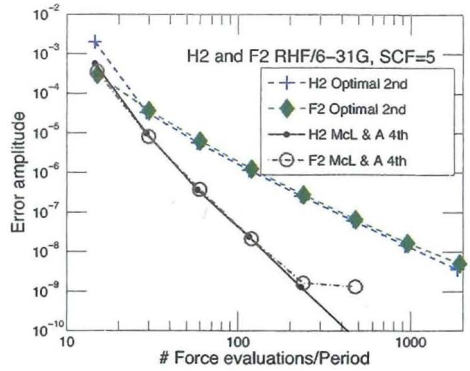

FIG. 3: The F_2 and H_2 molecules for the 2nd order optimal and 4th order McLachlan & Attela methods.

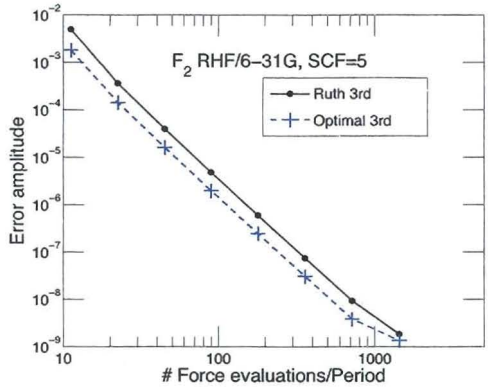

FIG. 4: F2 all 3rd order.

C. Performance over number of SCF cycles

The integrators with the smallest error for each order are also analyzed with regard to their behaviour for different number of SCF cycles in the SCF optimization loop. We do this to compare the error amplitude and slope for each integrator under different degrees of SCF convergence. The error amplitude for $1, 2$ and 5 SCF cycles have been evaluated. The result can be seen in figure 9-14. We find that the sensitivity in accuracy to the number of SCF cycles increases with the order of the integrators. This is because the higher-order methods require more accurate force evaluations to match ther higher-order accuracy level.

The higher order integrators give a very accurate propagation of the nuclear positions. However, for each new

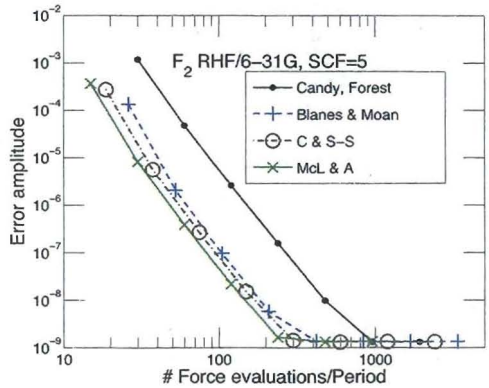

FIG. 5: F2 all 4th order.

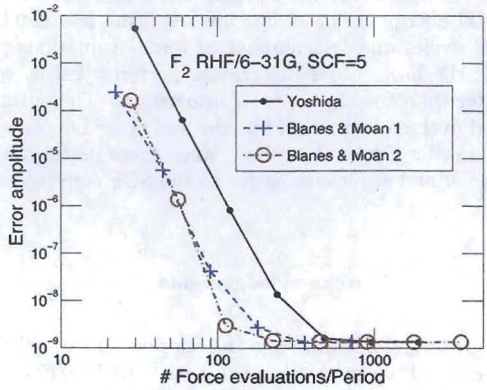

FIG. 6: F2 all 6th order.

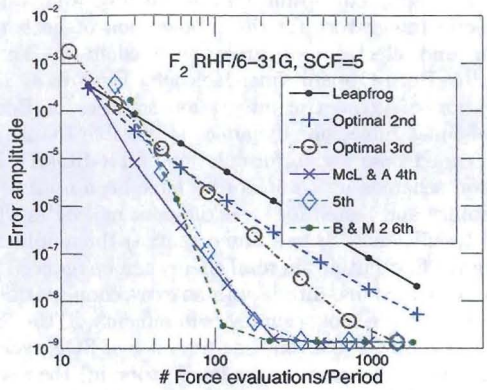

FIG. 7: Error amplitude as function of the number of force evaluations per period for all orders for the F_2 molecule.

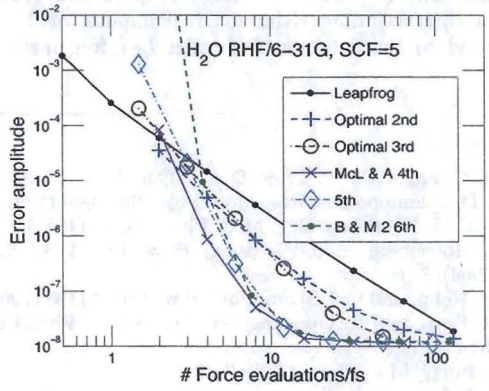

FIG. 8: Error amplitude as function of the number of force evaluations per unit time for all orders for the H_2O molecule.

nuclear configuration the electronic degrees of freedom have to be optimized to give the correct electrostatic forces. For few SCF cycles we get an approximate solution for the electronic degrees of freedom for the given nuclear configuration. In this case the full advantage of the higher degree of accuracy in higher order integrators is not made use of. For the higher order integrators, which gives a more accurate propagation of the nuclear configurations, more SCF cycles will bring us closer to the exact ground state, thus reducing the error amplitude. We can also see that the sensitivity of the number of SCF cycles increases with decreasing time step for all methods. The reason is the same as stated above. For a smaller time step we get a better propagation of the nuclear configuration, thus increasing the sensitivity for the number of SCF cycles. Because of this, the order of the convergence for the higher order methods (the slope of the ampliture error) also decreases with decreasing SCF convergence. The lower order methods (2nd and 3rd order) are very robust and the effect of a reduced degree of SCF convergence is small, Figs. (9), (10) and (11).

D. κ and SCF sensitivity

Integration schemes of the same order but with different κ values exhibit different amplitudes in the error. This is because schemes with a larger value for κ give a propagation of the auxiliary electronic variables P that is closer to the exact electronic ground state D in Eq. (7), (10) and (13). This is illustrated in figure 15 where the two different $6th$ order Blanes & Moan schemes are shown for a low level of SCF convergence. It is clear that the κ-value does not affect the order of convergence (the slope of the curve) but the amplitude of the error. The method with the largest κ value, Blanes & Moan 1 ($\kappa = 41.165$), has the smallest error amplitude. For higher SCF convergence, where the accuracy of the propagation of the electronic degrees of freedom is not as crucial, this effect is less strong. This can be seen in figure 6 where SCF = 5 and the two Blanes & Moan schemes are very close in the error amplitude.

V. SUMMARY

We have adapted, optmized, implemented and tested symplectic integrators for the propagation of both the nuclear and electronic degrees of freedom in Time-Reversible Born-Oppenheimer Molecular Dynamics. The application of geometric integration schemes in Born-Oppenheimer molecular dynamics is possible thanks to the extended Lagrangian formulation of TR-BOMD. Integration schemes up to $6th$ order have been optimized for stability and tested for three different molecules with regard to efficiency. It was found that: i) the amplitude of the error fluctuations in total energy can be reduced up to three orders of magnitude with no extra computational cost at high degrees of accuracy requirements; ii) the sensitivity of the SCF convergence (number of SCF cycles) increases with the order of the integrators; iii) the sensitivity of the SCF convergence increases with decreasing time step for all methods; iv) the order of convergence (slope of the curve) decreases with decreasing time step for low SCF convergence, especially for the higher order methods. This is a consequence of iii).

We can draw the conclusion that for calculations which require a high accuracy, using the Time Reversible BOMD method with a higher-order symplectic integrator, the time step can be increased up to two orders, with a corresponding reduction in computational cost compared to the common $2nd$ order Leapfrog method. In such cases we would recommend either of the $4th$ order McLachlan & Attela, the $5th$ order or the $6th$ order Blanes & Moan methods. For systems where the error in the total energy is not so crucial, requiring less number of SCF cycles and less number of force evaluations per period, the lower order integrators perform just as well or better than the higher order integrators. The optimal method in these cases would be the 2nd order Leapfrog or the 2nd order Optimal method, since these perform well at large δt and are less sensitive to the SCF convergence.

Acknowledgements

We gratefully acknowledge the support of the US Department of Energy through the LANL LDRD/ER program for this work. We also thank SNIC for computer resources and NSC for computer support. A special thanks goes to the people at the T-Division 10-Bar Java Group at Los Alamos National Laboratory for stimulating discussions, and to Travis Peery for his generosity and expertise.

VI. APPENDIX A

[1] M. C. Payne, M. P. Teter, D. C. Allan, T. A. Arias, and J. D. Joannopoulos, Rev. Mod. Phys. **64**, 1045 (1992).
[2] C. C. J. Roothaan, Rev. Mod. Phys. **23**, 69 (1951).
[3] P. Hohenberg, and W. Kohn, Phys. Rev **136**, B864 (1964).
[4] W. Kohn, and L. J. Sham, Phys. Rev. **140**, A1133 (1965).
[5] M. Born, and R. Oppenheimer, Annalen der Physik **84**, 457 (1927).
[6] P. Pulay, Mol. Phys. **17**, 197 (1969).
[7] P. Pulay and G. Fogarasi, Chem. Phys. Lett. **386**, 272 (2004).
[8] J. Herbert and M. Head-Gordon, Phys. Chem. Chem. Phys. **7**, 3269 (2005).
[9] T. Arias, M. Payne, and J. Joannopoulos, Phys. Rev. Lett. **69**, 1077 (1992).
[10] J. Millan, V. Bakken, W. Chen, L. Hase, and H. B. Schlegel, J. Chem. Phys. **111**, 3800 (1999).
[11] C. Raynaud, L. Maron, J.-P. Daudey, and F. Jolibois, Phys. Chem. Phys. **6**, 4226 (2004).
[12] A. M. N. Niklasson, C. J. Tymczak, and M. Challacombe, Phys. Rev. Lett. **97**, 123001 (2006).
[13] D. Frenkel and B. Smit, *Understanding Molecular Simulation* (Academic Press, 2002), 2nd ed.
[14] A. M. N. Niklasson, Phys. Rev. Lett. **100**, 123004 (2008).
[15] R. Ruth, IEEE Trans. Nucl. Sci. **30**, 2669 (1983).
[16] K. Feng, J. Comput. Math. **4**, 279 (1986).
[17] H. Yoshida, Phys. Lett. A **150**, 262 (1990).
[18] M. Tuckerman, B. J. Berne, and G. J. Martyna, J. Chem. Phys. **97**, 1990 (1992).
[19] *MondoSCF, http://www.t12.lanl.gov/home/mchalla/MondoSCF.*
[20] L. Verlet, Phys. Rev. **159**, 98 (1967).
[21] R. Car, and M. Parrinello, Phys. Rev. Lett. **55**, 2471 (1985).
[22] D. Marx and J. Hutter, *Modern Methods and Algorithms of Quantum Chemistry,* edited by J. Grotendorst (John von Neumann Institute for Computing, Jlich, Germany, 2000), 2nd ed.
[23] H. B. Schlegel, J. M. Millam, S. S. Iyengar, G.A. Voth, A. D. Daniels, G. Scusseria, and M. J. Frisch, J. Chem. Phys. **114**, 9758 (2001).
[24] J. M. Herbert and M. Head-Gordon, J. Chem. Phys **121**, 11542 (2004).
[25] S. Blanes, and P. C. Moan, Journ. of Comp. and Appl. Math. **142**, 313 (2002).
[26] R. I. McLachlan, and P. Atela, Nonlinearity **5**, 541 (1992).
[27] J. Candy, and W. Rozmus, Journ. of Comp. Phys. **92**, 230 (1991).
[28] E. Forest, and R. D. Ruth, Physica D **43**, 105 (1990).
[29] S. K. Gray, D. W. Noid, and G. Sumpter, J. Chem. Phys. **101**, 4062 (1994).
[30] D. Donnelly, E. Rogers, Am. J. Phys. **73**, 938 (2005).
[31] B. Leimkuhler, and S. Reich, *Simulating Hamiltonian Dynamics* (Cambridge University Press, Cambridge, England, 2004)

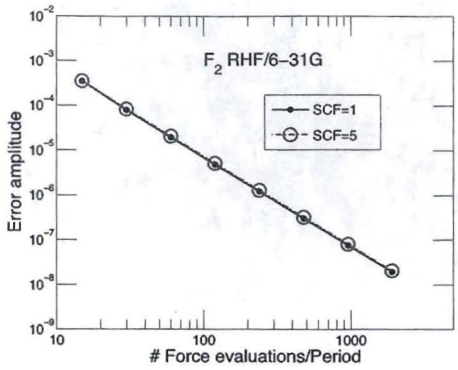

FIG. 9: Leapfrog $\kappa = 2$

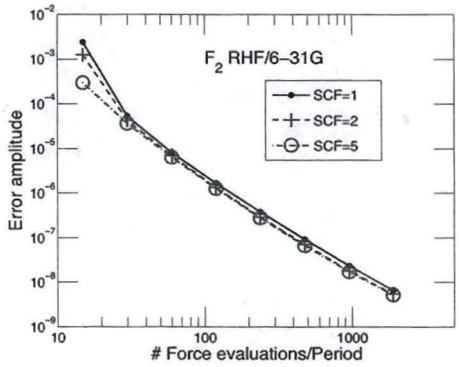

FIG. 10: Optimal 2nd order.
$\kappa = 2.563$

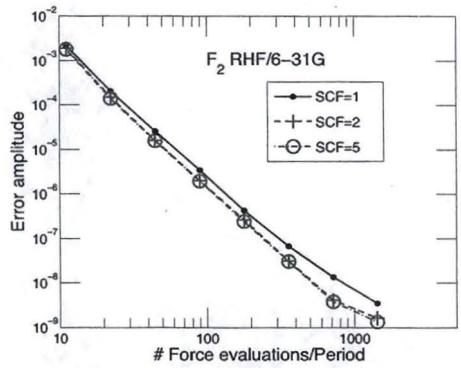

FIG. 11: Optimal 3rd order.
$\kappa = 10.215$

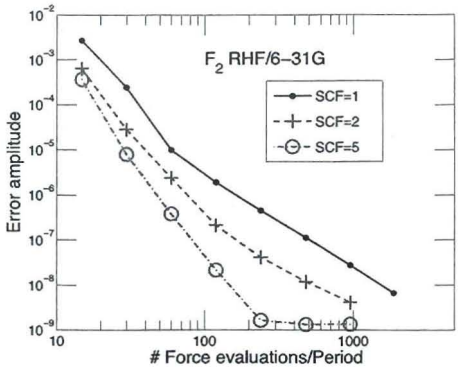

FIG. 12: 4th order McLachlan
Atela. $\kappa = 4.617$

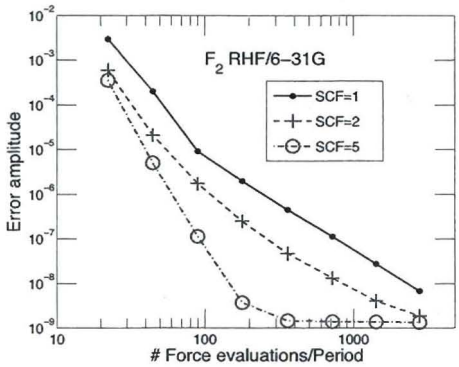

FIG. 13: 5th order. $\kappa = 4.6894$

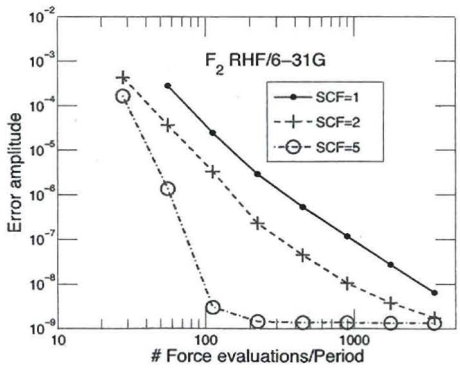

FIG. 14: 6th order Blanes
Moan 2. $\kappa = 18.911$

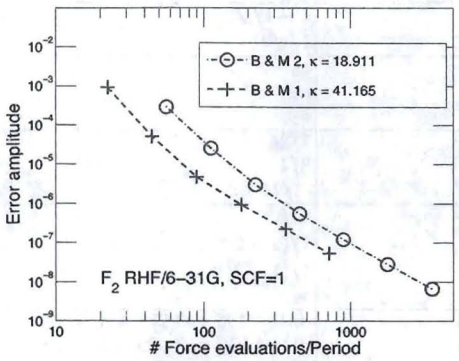

FIG. 15: The Blanes & Moan 6th order methods with 1 SCF cycle.

Name	Ref.	Order	a	b
Leapfrog	[26]	1	1/2	0
			1/2	1
Optimal 2nd	[26]	2	$1/\sqrt{2}$	$1-1/\sqrt{2}$
			$1-1/\sqrt{2}$	$1/\sqrt{2}$
Optimal 3rd	[26]	3	0.919661523017400	a_3
			$1/(4a_1)-a_1/2$	a_2
			$1-a_1-a_2$	a_1
Ruth 3rd	[15]	3	2/3	7/24
			-2/3	3/4
			1.0	-1/24
Candy, Forest	[27, 28]	4	$1/6(2+2^{1/3}+2^{-1/3})$	0.0
			$1/6(1-2^{1/3}-2^{-1/3})$	$1/(2-2^{1/3})$
			a_2	$1/(1-2^{1/3})$
			a_1	b_2
McLachlan & Atela	[26]	4	0.515 352 837 431 122 936 4	0.134 496 199 277 431 089 2
			-0.085 782 019 412 973 646	-0.224 819 803 079 420 805 8
			0.441 583 023 616 466 524 2	0.756 320 000 515 668 291 1
			0.128 846 158 365 384 185 4	0.334 003 603 286 321 425 5
Calvo & Sanz-Serna	[29]	4	0.205 177 661 542 290	0.061 758 858 135 626
			0.403 021 281 604 210	0.338 978 026 553 64
			-0.120 920 876 338 91	0.614 791 307 175 58
			0.512 721 933 192 410	-0.140 548 014 659 37
			0.0	0.125 019 822 794 53
Blanes & Moan	[25]	4	0.082 984 406 417 405 2	0.245 298 957 184 271
			0.396 309 801 498 368	0.604 872 665 711 080
			-0.039 056 304 922 348 6	$1/2-(b_1+b_2)$
			$1-2*(a_1+a_2+a_3)$	b_3
			a_3	b_2
			a_2	b_1
			a_1	0.0
5th	[26]	5	0.339 839 625 839 110 000	0.119 390 029 287 567 275 8
			-0.088 601 336 903 027 329	0.698 927 370 382 475 230 8
			0.585 856 476 825 962 118 8	-0.171 312 358 271 600 775 4
			-0.603 039 356 536 491 888	0.401 269 502 251 353 448 0
			0.323 580 796 554 697 639 4	0.010 705 081 848 235 984 0
			0.442 363 794 219 749 458 7	-0.058 979 625 498 031 163 2
Blanes & Moan 1	[25]	6	0.041 464 998 518 262 4	0.123 229 775 946 271
			0.198 128 671 918 067	0.290 553 797 799 558
			-0.040 006 192 104 153 3	-0.127 049 212 625 417
			0.075 253 984 301 580 7	-0.246 331 761 062 075
			-0.011 511 387 420 687 9	0.357 208 872 795 928
			$1/2-(a_1+a_2+a_3+a_4+a_5)$	$1-2*(b_1+b_2+b_3+b_4+b_5)$
			a_6	b_5
			a_5	b_4
			a_4	b_3
			a_3	b_2
			a_2	b_1
			a_1	0.0
Blanes & Moan 2	[25]	6	0.037 859 319 840 611 6	0.091 719 152 624 461 65
			0.102 635 633 102 435	0.183 983 170 005 006
			-0.025 867 888 266 558 7	-0.056 534 365 832 888 27
			0.314 241 403 071 447	0.004 914 688 774 712 854
			-0.130 144 459 517 415	0.143 761 127 168 358
			0.106 417 700 369 543	0.328 567 693 746 804
			-0.008 794 243 128 510 58	$1/2-(b_1+b_2+b_3+b_4+b_5+b_6)$
			$1-2*(a_1+a_2+a_3+a_4+a_5+a_6+a_7)$	b_7
			a_7	b_6
			a_6	b_5
			a_5	b_4
			a_4	b_3
			a_3	b_2
			a_2	b_1
			a_1	0.0
Yoshida	[17]	6	$1/2*c_3$	c_3
$c_1=0.152886228424922*10^{-2}$			$1/2*(c_3+c_2)$	c_2
$c_2=-0.214403531630539*10^{1}$			$1/2*(c_2+c_1)$	c_1
$c_3=0.144778256239930*10^{1}$			$1/2*(c_1+c_4)$	c_4
$c_4=1-2*(c_1+c_2+c_3)$			a_4	c_1
			a_3	c_2
			a_2	c_3
			a_1	0.0

TABLE II: Coefficients for symplectic integrators.